Quantifying the failure probability of a canal levee

Lendering, K.; Schweckendiek, T.; Kok, Matthijs

DOI
10.1080/17499518.2018.1426865

Publication date
2018

Document Version
Final published version

Published in
Georisk: assessment and management of risk for engineered systems and geohazards

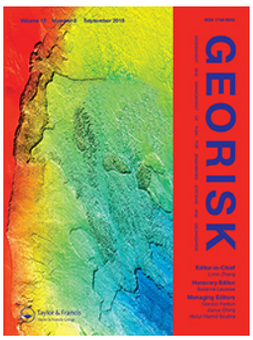

Taylor & Francis
Taylor & Francis Group

Georisk: Assessment and Management of Risk for Engineered Systems and Geohazards

ISSN: 1749-9518 (Print) 1749-9526 (Online) Journal homepage: https://www.tandfonline.com/loi/ngrk20

Quantifying the failure probability of a canal levee

K. Lendering, T. Schweckendiek & M. Kok

To cite this article: K. Lendering, T. Schweckendiek & M. Kok (2018) Quantifying the failure probability of a canal levee, Georisk: Assessment and Management of Risk for Engineered Systems and Geohazards, 12:3, 203-217, DOI: 10.1080/17499518.2018.1426865

To link to this article: https://doi.org/10.1080/17499518.2018.1426865

Published online: 22 Jan 2018.

GEORISK, 2018
VOL. 12, NO. 3, 203–217
https://doi.org/10.1080/17499518.2018.1426865

Taylor & Francis
Taylor & Francis Group

Quantifying the failure probability of a canal levee

K. Lendering, T. Schweckendiek and M. Kok

Faculty of Civil Engineering and Geosciences, Delft University of Technology, Delft, Netherlands

ABSTRACT

Polders in the Netherlands are protected from flooding by flood defence systems along main water bodies such as rivers, lakes or the sea. Inside polders, canal levees provide protection from smaller water bodies. Canal levees are mainly earthen levees along drainage canals that drain excess water from polders to the main water bodies. The water levels in these canals are regulated. During the last decades, probabilistic approaches have been developed to quantify the probability of failure of flood defences along the main water bodies. This paper proposes several extensions to this method to quantify the probability of failure of canal levees. These extensions include a method to account for (i) water-level regulation in canals, (ii) the effect of maintenance dredging on the geohydrological response of the canal levee and (iii) survival of loads in the past. The results of a case study demonstrate that the proposed approach is capable of quantifying the probability of failure of canal levees and is useful for exploring the relative benefit of risk mitigating measures for canal levees.

ARTICLE HISTORY
Received 3 May 2017
Accepted 29 December 2017

KEYWORDS
Canal levee; flood risk analysis and management; reliability analysis; quantitative risk analysis

1. Introduction

Polders are often built in river deltas or in low-lying coastal areas to reclaim land. In the Netherlands, a large part of the country consists of polders, but polders are also found in Belgium, New Orleans, Sacramento or Bangkok. Polders typically lie below the surrounding water and are protected from flooding from the main water bodies by flood defences. These flood defences protect polders from the main hazards such as riverine or coastal flooding. Within these polders, large storage and drainage systems are made to drain excess water from the polders to the main water bodies. The drainage canals are aligned by canal levees that protect the surrounding polder from flooding from the inner water (inside the drainage and storage areas).

Traditionally, the strength of flood defences in the Netherlands is assessed using a semi-probabilistic approach (with safety factors) based on a statistically defined water level. In the last decades, full probabilistic approaches have been developed to assess the failure probability of flood defence systems accounting for the variability and uncertainty in both load and strength. The latter approach was used to quantify the probability of failure of flood defences along the main water bodies in the Netherlands, in the project "Flood Risk of the Netherlands" (Jongejan, Maaskant, and Ter Horst 2013; Vrijling 2001). The results of the project provided input for new safety standards for flood defences in the Netherlands (Rijkswaterstaat 2015), both in terms of cost-effectiveness of flood mitigation measures as well as considering risk to life (Jonkman 2005; Jonkman and Kok 2008; Slijkhuis, van Gelder, and Vrijling 2001).

Canal levees were not taken into account in the VNK2 project, even though there are several polders in the Netherlands with significant risk of flooding from the inner water bodies inside polders. For example, critical infrastructure such as the international airport of Schiphol and the high-speed rail line are both situated inside the Haarlemmermeerpolder, which is surrounded by a canal levee that aligns a large drainage canal system. Flooding from this canal system can result in significant (economic) flood damage. Furthermore, the dike breach at Wilnis in 2003 demonstrated that canal levees can breach at unexpected moments, in this case during a period of long drought in summer (Van Baars and Van Kempen 2009). Currently, the strength of canal levees is still assessed using a semi-probabilistic approach. The development of a full probabilistic approach can contribute to more effective flood risk management in areas at risk from flooding due to

CONTACT K. Lendering k.t.lendering@tudelft.nl Faculty of Civil Engineering and Geosciences, Delft University of Technology, Stevinweg 1, 2628CN Delft, Netherlands

Supplemental data for this article can be accessed at doi:10.1080/17499518.2018.1426865

water bodies inside polders. This full probabilistic approach needs to take into account aspects specific to canal levees (and different from other flood defences), such as the regulation of water levels in canals and the occurrence of multiple loads on canal levees (e.g. water levels, rainfall and traffic loads).

This paper proposes an extension of the approach to quantify the probability of failure of flood defences along the main water bodies to enable reliability analysis of canal levees. The application to the canal levee requires several additional features to account for (i) regulation (and drainstop) of water levels in canals, (ii) the possibility of (removal of) hydraulic resistance on the bottom of the canal due to maintenance dredging, (iii) the uncertainty in traffic loads and iv) the uncertainty of the phreatic surface. The paper is based on a more extensive technical report; more information on the discussed framework and case studies can be found in Lendering, Jonkman, and Kok (2015). It is built up as follows. Section 2 describes the method proposed to quantify the probability of failure of a canal levee. In Section 3, we apply the method to a case study in the Netherlands. Finally, Section 4 contains the conclusions and recommendations.

2. Failure probability assessment

2.1. System description

Polders often lay below the main water bodies (e.g. a river, lake or sea) and are temporarily or permanently at risk of flooding. Water enters polders through groundwater flow and/or precipitation. Excess water is drained to the main water bodies through a drainage canal system. These drainage canals serve as temporary storage before the water is ultimately drained to the main water bodies. A schematised cross section of such a system is shown in Figure 1. Drainage canals are typically aligned by canal levees. Traditionally, these canal levees were constructed from locally available soil, often a mixture of clayey and peaty material. Seepage through the levees or bottom of the canal is limited due to the low conductivity of the materials used. Canal levees often are also used for roads.

The following Section 2.2 discusses the general approach used to quantify the probability of failure of canal levee systems. The main loads on canal levees are discussed in Section 2.3, followed by a description of the considered failure mechanisms and how their probability is quantified in Section 2.4. Finally, Section 2.5 discusses a method to update the probability of failure using performance observations.

2.2. General approach

This paper focusses on quantifying the probability of failure of canal levees. To this purpose, we will use the full probabilistic approaches applied in the VNK2 project (Jongejan, Maaskant, and Ter Horst 2013). An assessment of the consequences of flooding of canal levees and corresponding risk of flooding is beyond the scope of this paper, but is treated in Lendering, Kok, and Jonkman (2015).

The canal levee system is divided in sections with distinct, but homogeneous, strength properties, which allows independent modelling of sections in terms of strength. Failure is defined as breaching of the canal levee and occurs when the load (S) exceeds the resistance (R). For example, a canal levee fails when the water level in the canal (i.e. the load) exceeds the retaining height of the levee (i.e. the resistance).

Limit state functions (Z) are defined for the dominant failure mechanisms of the considered canal levee. The limit state describes the condition beyond which the levee fails – in other words, the condition beyond which the resistance no longer exceeds the load. The general form of a limit state function is shown in Equation (1), where the loads are described by the *Solicitation* (S) and the strength by the *Resistance* (R). The probability of the considered failure mechanism is quantified

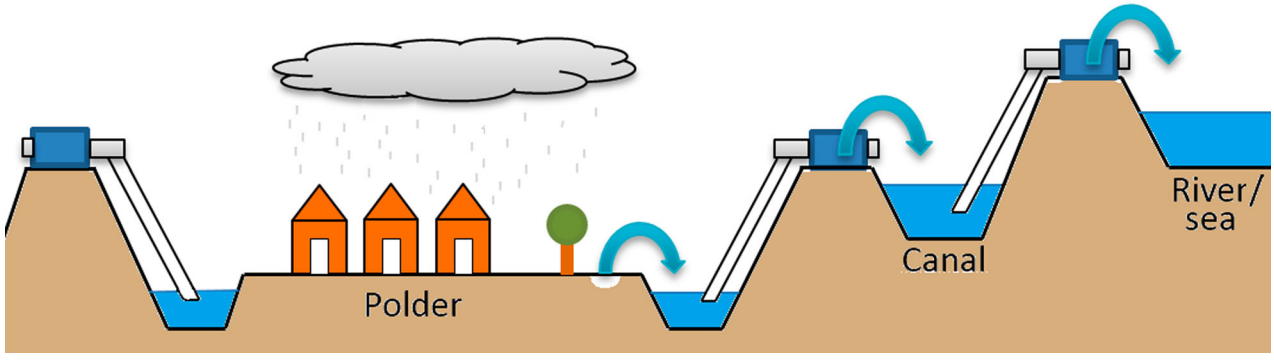

Figure 1. Typical cross section of a polder.

by the probability that the limit state function (Z) is smaller than zero (Equation (2)).

$$Z = \text{Resistance} - \text{Solicitation}, \quad (1)$$

$$P_f = P(Z(x) < 0) = P(Z(R, S) < 0). \quad (2)$$

The cumulative distribution function (CDF) of the strength ($F_r(s)$) represents the conditional probability of failure mechanisms upon loading. Fragility curves illustrate the resulting conditional failure probability for the considered failure mechanism and load. These curves can be multidimensional depending on the number of loads considered (Vorogushyn, Merz, and Apel 2009). Through integration of the CDF of the strength ($F_r(s)$) over the probability density function (PDF) of the considered load ($f_s(s)$), we can determine the total yearly probability of the considered failure mechanism (Equation (3)).

$$P_f = \int_{r=-\infty}^{r=\infty} \int_{s=-\infty}^{s=\infty} f_{r,s}(r, s)\mathrm{d}r\,\mathrm{d}s = \int_{s=-\infty}^{s=\infty} f_s(s) \cdot F_r(s)\mathrm{d}s. \quad (3)$$

This equation is not solved analytically because limit state functions of failure mechanisms are complex functions that can only be solved in a limited number of simple cases (Gouldby et al. 2008). Therefore, we propose to determine the CDF of the strength for a discretized set of load levels (E_j) using Level III (Monte Carlo simulations) and/or Level II (first-order approximation) probabilistic methods. The total failure probability is found after integrating the CDF of the strength over the PDF of the loads, taking into account dependence between the considered loads. Depending on the considered loads, different load scenarios with corresponding probabilities are taken into account using the law of total probability:

$$P_f = P(Z(x) < 0) = \sum_j P(f\,|E_j) \cdot P(E_j). \quad (4)$$

Observations of survived loads along these canal levees provide valuable information of the strength of the levee. These performance observations can be used to reduce uncertainties of the strength of the levee and therefore reduce the failure probability (Schweckendiek, Vrouwenvelder, and Calle 2014). After calculation of the probability of each failure mechanism, we will demonstrate how performance observations (survived loads) can be used to update the failure probabilities.

The probability of failure of the considered levee section is found by a combination of the probability of each failure mechanism, taking dependence into account. The upper and lower bounds of the failure probability are found by assuming mutually exclusive (upper bound) or complete dependence (lower bound) between failure mechanisms, see Equation (5). In this equation, "i" represents each considered geotechnical failure mechanism and "n" represents the total amount of failure mechanisms considered.

$$\underset{i=1}{\overset{n}{\mathrm{MAX}}} P_{f;i} \le P_{f;\mathrm{sys}} \le \sum_{i=1}^{n} P_{f;i}. \quad (5)$$

Based on experience obtained in the VNK2 project (Jongejan, Maaskant, and Ter Horst 2013), we assume independence between failure mechanisms, allowing us to use Equation (6) to calculate the probability of failure of the system. This assumption will be discussed further in the case study.

$$P_{f;\mathrm{sys}} = 1 - \prod_{i=1}^{n} (1 - P_{f;}i). \quad (6)$$

2.3. Main loads on canal levees

This section discusses the uncertainties of the main loads on the canal levees, being hydraulic (e.g. water levels) and traffic loads. Uncertainties are typically characterised by extreme value distributions. The main hydraulic loads consist of the water levels in the drainage canals and the phreatic surface in the canal levee (which influences the stability of the levee). Wave loads can generally be neglected, as the fetch on canals is typically insufficient to generate significant wind waves. Maintenance dredging can (unintentionally) increase the infiltration capacity of the bottom of the canal, resulting in increased porewater pressure in the aquifer under the levee.

An overview of the main loads is shown in Figure 2. In our approach, the continuous PDFs of these load variables are discretized in a predefined set of plausible load levels with corresponding probability density.

2.3.1. Water levels

Water levels in canals are influenced by inflow from the polder drainage stations, direct precipitation and drainage to the main water bodies. The water level in these drainage canals is regulated at a target level, which lies above the surrounding polders (see Figure 2). This target

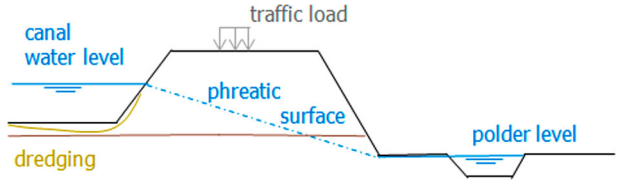

Figure 2. Cross section of a canal levee, illustrating the main loads acting on a canal levee.

level is determined by a minimum required drainage or storage capacity in the canal or by other practical requirements, such as a minimum required navigation depth.

Besides the target level, a maximum target level is typically defined: the so-called drainstop level, whose aim is to prevent extreme water loads on the canal levees. During heavy precipitation events, the pumping stations stop draining water from the polder to the drainage canal once the water level in the canal reaches the drainstop level, or maximum target level. The difference between the target level and the drainstop level is typically in the order of decimetres. Failure of the drainstop, i.e. failure of water-level regulation (e.g. because local water authorities neglect, or forget, to turn off the pumping stations once the maximum target level is reached), can result in water levels exceeding the drainstop level.

A Generalised Pareto Distribution (GPD) is fitted to water-level data to obtain the probability distribution (f_{GPD}) of the annual maximum water levels in the canal. In case of a perfectly working drainstop, the GDP would be truncated at the drainstop level and represented by ($f_{\mathrm{drainstop}}$) in Figure 3. To account for water-level regulation failures, a combined probability distribution ($f(h)$) of the canal water level is generated using the law of total probability, as defined in Equation (7):

$$f(h) = P_{f;\mathrm{drainstop}} \cdot f_{GPD} + (1 - P_{f;\mathrm{drainstop}}) \cdot f_{\mathrm{drainstop}}. \quad (7)$$

Here, ($P_{f;\mathrm{drainstop}}$) is the probability of failure of the drainstop ($P_{f;\mathrm{drainstop}}$) that can be estimated by the annual frequency of water-level observations that exceeded the "drainstop level" (λ) using Equation (8). An alternative to this empirical method is to determine the failure probability of the drainstop with a full reliability analysis taking human error into account, an example of such an analysis for emergency measures is given in Kirwan (1996) and Lendering, Jonkman, and Kok (2015).

$$P_{f;\mathrm{drainstop}} = 1 - e^{-\lambda t} \text{ with } (t = 1 \text{ year}). \quad (8)$$

2.3.2. Phreatic surface

Without infiltration or evaporation, the phreatic surface inside the levee will reach a steady state: the canal-side boundary of the phreatic surface depends on the water level in the canal, while the land-side boundary of the phreatic surface depends on the water level in the polder. Rainfall (infiltration) and drought (evaporation) influence the saturation and, hence, the phreatic surface in time. The impact depends (among others) on the type of soil, the geometry of the levee and meteorological aspects (e.g. air moisture). Finally, the pore pressures induced by groundwater reduce the effective stresses in the soil and thereby the stability of the inner slope.

Groundwater flow models and/or monitoring of the groundwater table inside the canal levee can provide insight into the response of the phreatic surface to different forcing scenarios (e.g. heavy precipitation) with corresponding probability. However, research suggests that although different groundwater flow models can produce similar results, it remains difficult to reproduce observed groundwater levels (Van Esch 2012) and it is even more difficult to predict them. One main reason for the difficulty to model pore pressures by seepage analysis is the uncertainty in initial conditions in terms of the degree of saturation and the phreatic surface in daily conditions. Soil–atmosphere interaction in terms of precipitation and evaporation often results in groundwater trapped in the levee, at least in peat levees. At the same time, these processes are difficult to capture accurately in seepage analyses. Therefore, expert estimates based on

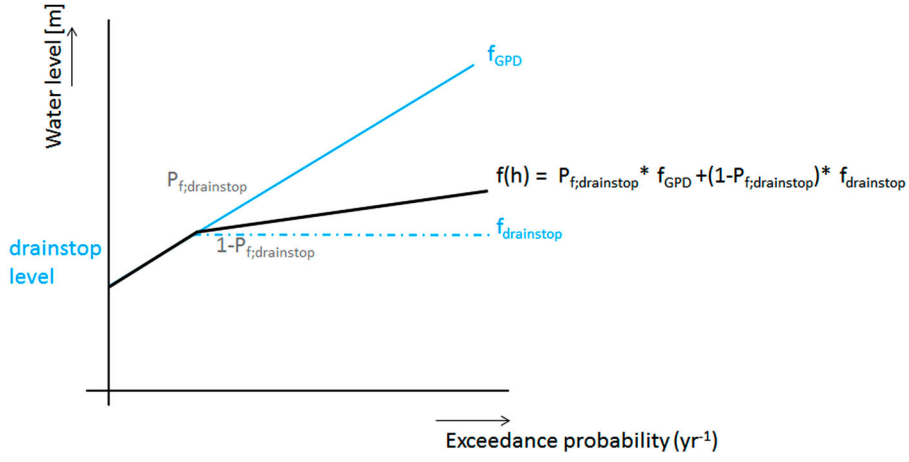

Figure 3. Annual exceedance frequency model of canal water levels.

experience with monitored or measured similar conditions are often as reliable as the results of seepage analyses. As for monitoring, the considered canal systems typically consist of tens or hundreds of kilometres of levee. Monitoring over the entire length of the system is typically not economically feasible. The expert judgment-based approach should provide a reasonable first estimate in data-scarce conditions and the results can be perfectly used to target monitoring efforts to the risk hotspots.

Our specific, pragmatic proposal is to discretize the PDF of the phreatic surface as a set of plausible levels dependent on two canal water levels: an average water level and an extreme water level (e.g. the drainstop level). A typical discretization contains three levels for the phreatic surface: low, average and high.

- A low level corresponds with a dry period, which may occur when the water levels in the canal are very low during a period of drought (no precipitation).
- An average level corresponds to the steady state situation with water levels at the target level.
- A high level corresponds to a situation where the levee is saturated, which may occur due to an extreme water level in the canal and/or during extreme precipitation.

With average canal water levels, the phreatic surface will likely be close to its steady state. In contrast, with extreme water levels, which are the result of heavy precipitation, a high phreatic surface is most likely. The corresponding conditional probabilities can be estimated by, for example, members of water boards involved with the day-to-day maintenance of canal levees and often with knowledge of monitoring data from similar conditions.

2.3.3. Traffic loads

The combination of extreme hydraulic and traffic loads can be governing for the stability of a canal levee. Traffic loads are currently taken into account deterministically as a static vertical load on top of the canal levee. We propose a probabilistic approach taking both the uncertain presence of the traffic load and the uncertainty of the magnitude of the traffic load into account.

The presence of a traffic load on the canal levee depends on the considered canal levee (e.g. are there roads on top) and if flood fighting activities are expected during emergencies (e.g. will the local water board place sandbags on top of the levee to increase its height). To take this into account, we will estimate the conditional probability of failure of the canal levee with ($P_{f;\text{inst}|\text{tl}}$) and without a traffic load ($P_{f;\text{inst}|\overline{\text{tl}}}$) during all hydraulic loads, and use the law of total probability to account for the probability of traffic loads (P_{tl}).

$$P_{f;\text{inst}} = P_{f;\text{inst}|\text{tl}} \cdot P_{\text{tl}} + P_{f;\text{inst}|\overline{\text{tl}}} \cdot P_{\overline{\text{tl}}} \text{ with } P_{\overline{\text{tl}}} = 1 - P_{\text{tl}}. \tag{9}$$

According to the guidelines for assessment of canal levees in the Netherlands (Stowa 2007), a static traffic load of 13.3 kN/m^2 over a width of 2.5 m in a plain-strain analysis needs to be taken into account. This is the equivalent of a 12-m-long, 40 ton vehicle. The effect of dynamic loads is assumed negligible in this study. For the purpose of modelling the traffic load probabilistically, water board employees were asked to provide estimates of the magnitude of average and extreme traffic loads, this is treated in more detail in Section 3.

2.4. Limit states of failure mechanisms

The probability of failure of canal levees is typically dominated by the probability of overflowing, instability and/or piping, whereas the contributions of other mechanisms such as instability of the revetment or wave overtopping are typically negligible (no significant wave action) (Figure 4).

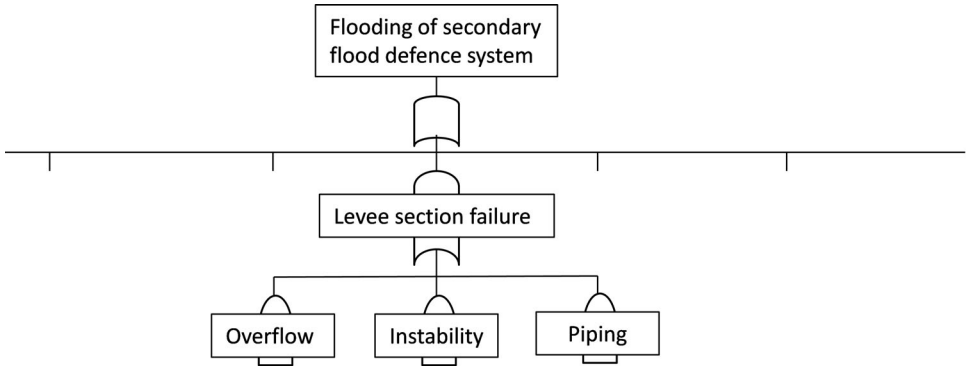

Figure 4. Simplified fault tree for the governing failure mechanisms of a canal levee section: overflow, instability and piping.

The limit state functions of the governing failure mechanisms are described in the following sections, followed by a description of how to quantify the probability of each mechanism. Fault tree analysis is used to combine the probability of each mechanism and quantify the failure probability of the considered canal levee section.

2.4.1. Overflow

Overflow occurs when the water levels in the canal (H_w) exceed the retaining height (crest level) of the levee (H_r), causing erosion of the inner slope. The limit state function (Z_{overflow}) considers a critical overflow height (Δh_c), derived from a critical flow (q_c) that leads to erosion of the inner slope and ultimately breaching, see Ciria (2014).

$$Z_{\text{overflow}} = H_r + \Delta h_c - H_w \text{ with } :\Delta h_c = \sqrt[3]{\frac{q_c^2}{0.36g}}. \quad (10)$$

Note that the duration of overflow determines whether or not breaching of the considered levee will occur. In this paper, we neglect the duration of overflow (which could amount up to several days) and assume failure to correspond with exceedance of the critical overflow height.

2.4.2. Piping

Piping occurs when the head difference over a levee causes internal erosion inside or through the body of a levee, which is the result of soil particles that are carried downstream by seepage flow. This can cause the formation of channels that undermine the levee and can ultimately cause breaching (Ciria 2014). The probability of piping depends on the head difference over the canal levee, which is the difference between the water level in the canal (H_w) and the polder level (H_i). The limit state function for piping considers a critical head difference (H_p), which is calculated with the updated Sellmeijer formula (Sellmeijer et al. 2011). Note that this formula is only applicable to loads with long durations, which is relevant for canal levees due to the regulation of water levels, but may not be applicable to other situations (e.g. river floods).

The water in the drainage canals is not always in direct contact with the aquifer below the canal levee; seepage to the surrounding polder is limited due to the low conductivity of the clayey/peat layers on the bottom of the canals. This so-called hydraulic resistance increases the resistance against piping. To account for hydraulic resistance, a variable (H_{ir}) is included in the limit state function of piping that effectively reduces the hydraulic head over the canal levee. The complete limit state function for piping is described by Equation (11). The thickness of the blanker layer behind the levee is modelled by variable (D_0). The model parameter (m_b) takes into account model uncertainty.

$$Z_p = m_b \cdot H_p - (H_w - 0.3 \cdot D_0 - H_i - H_{ir}). \quad (11)$$

The hydraulic resistance can be removed (temporarily) due to regular maintenance dredging of the canals, because dredging activities effectively remove the impermeable layers on the bottom of the canals. The probability of piping is estimated conditional on the hydraulic resistance, after which an estimate is made of the probability of removal of hydraulic resistance ($P_{\overline{ir}}$) based on the frequency of dredging activities and its impact (depth). The conditional probability of piping hydraulic can be determined through Monte Carlo simulation or other reliability analysis techniques. The total probability of piping ($P_{f;p}$) is found after combining the conditional probability of piping given hydraulic resistance ($P_{f;p|ir}$) and removal of the hydraulic resistance ($P_{f;p|\overline{ir}}$), taking into account the probability of hydraulic resistance (P_{ir}) (using Equation (12)).

$$P_{f;p} = P_{f;p|ir} \cdot P_{\overline{ir}} + P_{f;p|\overline{ir}} \cdot P_{ir} \text{ with } P_{\overline{ir}} = 1 - P_{ir}. \quad (12)$$

2.4.3. Inner slope instability

Inner slope instability occurs when critical soil masses slide of the inner slope of the canal levee. The Bishop (1955) method is used to calculate the stability of the inner slope, for which the software D-Geo Stability (Deltares 2016) is used to determine the probability of failure. D-Geo Stability uses first-order approximation methods to determine the probability of inner slope failure conditional on a deterministic combination of the canal water level, the phreatic surface and the traffic load. Only slip circles that protrude the crest of the canal levee are taken into account, as only these are considered to lead to breaching of the levee. The uncertainties in strength properties are based on the default values used in the VNK2 project (Jongejan, Maaskant, and Ter Horst 2013).

The total probability of inner slope instability is determined after integration of the conditional failure probabilities over the joint probability distribution function of the considered loads. Assumptions regarding dependence between loads are discussed in the case study.

2.5. Using performance observations to update failure probabilities

Performance observations, such as the survival of extreme loads, can be used for reducing the uncertainty in a levee's strength (Schweckendiek 2014). Along

canal levees, the difference between average loads (e.g. the target water level) and extreme loads (e.g. the drainstop level) are typically limited to several decimetres, due to the regulation of water levels. Survived water levels near (or over) the drainstop level can provide valuable information. This information can be used to reduce strength uncertainties and update failure probabilities in a posterior analysis (also called Bayesian Updating).

Bayes' Rule forms the basis for updating probabilities with evidence of survived loads, see Equation (13), where F is the failure event to be predicted (i.e. $Z < 0$) and ε the observed event or evidence of the survived load (Schweckendiek 2014).

$$P(F|\varepsilon) = \frac{P(Z(x) < 0 \cap h(x) < 0)}{P(h(x) < 0)}. \qquad (13)$$

The observation ε is described by the exceedance of an observational limit state expressed with an observational limit state function $h(x)$, where (h) needs to be defined such negative values implies the observation to be true – in our case survival of the observed load. In the posterior analysis we assume the strength parameters to be time invariant and, hence, fully correlated between the survived and the predicted event. More details regarding the steps used in the prior and subsequent posterior analysis are described in Schweckendiek, Vrouwenvelder, and Calle (2014).

The effectiveness of a posterior analysis largely depends on the availability, accuracy and reliability of data of historically survived loads (ENW 2009). The potential influence of the posterior analyses on the failure probability increases when the survived loads or load effects (i.e. the survived water level) approach the extreme loads or load effects.

3. Case study in the "Heerhugowaard polder"

3.1. Case description

The approach described hitherto is applied to a system of canal levees surrounding a polder in the western part of the Netherlands. The polder is named the "Heerhugowaard" after the city that lies within (see Figure 5). The polder is surrounded by two large drainage canals that drain excess water from the polders to the North Sea: the "Schermer" and the "Verenigde Raaksmaats- en Niedorperkoggeboezem" (VRNK) canal. The 32 km long levee system is divided into six reaches for the purpose of flood risk analysis. Each reach consists of several sections as illustrated in Figure 5. In a flood risk analysis, the probability of failure of all sections within one reach would need to be combined to obtain the probability of flooding of the considered reach (i.e. a breach within the reach). The locations of four pumping stations along the levee system are also shown.

3.2. Load uncertainties

In our proposed approach, we estimated the PDFs of the phreatic surface and traffic loads in a "base case". Additionally, we performed sensitivity analyses to investigate the sensitivity of the probability of instability to these estimates. The following subsections discuss the

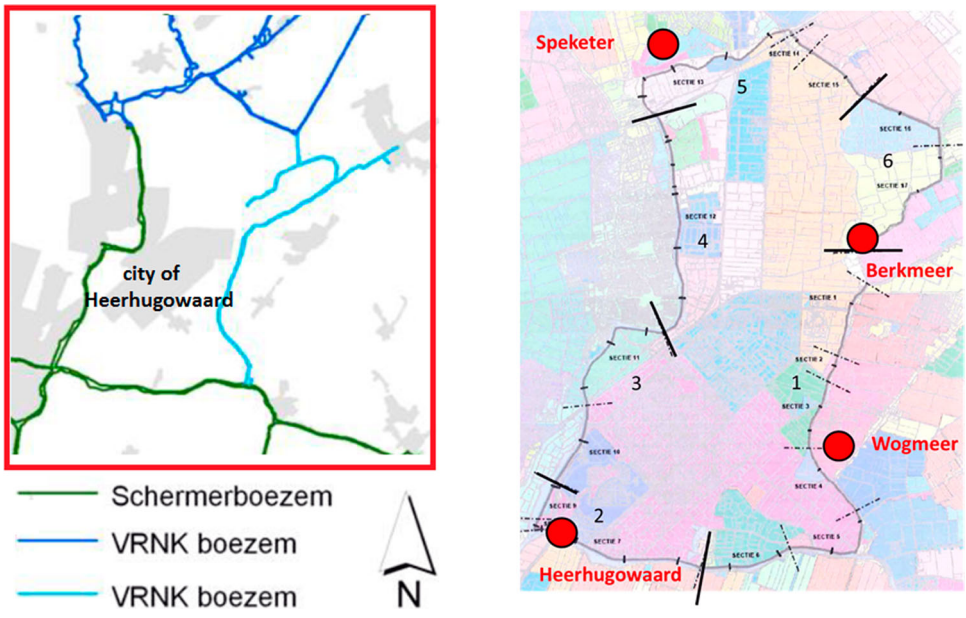

Figure 5. Overview of the Heerhugowaard polder surrounded by the Schermer and VRNK canals (left) and plan view of schematisation of levee system including pumping stations (Lendering, Kok, and Jonkman 2015).

PDFs of the water levels in the canal, the phreatic surface and traffic loads.

3.2.1. Water level

This section describes the probabilistic load models for the case study as described in general terms in Section 2.3. The annual exceedance lines of the canal water level are determined using water-level observations in the Schermer and VRNK canal. A GPD is fitted through independent water-level peaks after which the probabilities were corrected for the annual frequencies to obtain an annual exceedance line of water levels of the canal (Figure 6). Water levels are noted in metres relative to "Normaal Amsterdams Peil" or NAP.

The drainstop level of each canal is shown in Table 1 and Figure 7. In the Netherlands, the water boards define the drainstop level by a target annual probability of exceedance of 1/100, which means that the annual probability of excess water in polders due to pluvial flooding is 1/100. However, the data of observed water levels shows that this target is not always met. In the considered case study, we used the observed frequency of exceedance of the drainstop level to obtain an estimate of the probability of exceedance of the drainstop level.

The dataset for the Heerhugowaard station was limited to eight years, during which the drainstop level was never exceeded. Based on this data, no reliable estimate of the probability of exceedance could be made for this location. In the absence of more data, for this canal we assume that the target annual probability is met. We therefore assume an annual probability of exceedance of 1/100 for the Schermer canal and 1/9 for the VRNK canal (based on the observations in that canal). On the VRNK canal, the dataset for the Wogmeer station was limited to 22 years during which the drainstop level was exceeded several times. The combined annual exceedance frequency model of the water level of both canals, according to the approach described in Section 2, is shown in Figure 7.

3.2.2. Phreatic surface

In Section 2, we proposed a discretized set of phreatic surfaces, conditional on the canal water level, that contains three levels: low, average and high. The correlation between both loads is determined by the amount and duration of precipitation within the canal system. The (simultaneous) response of the canal level and phreatic surface to precipitation depends on the size of the considered canal system and the properties of the considered canal levee (e.g. the infiltration capacity).

In the absence of monitoring data, we assume a "base case" with a positive correlation between the canal water level and the phreatic surface, as described in the following bullets:

- Given an average canal water level: it is most likely that the phreatic surface reaches a steady state between the canal side and polder side of the levee.

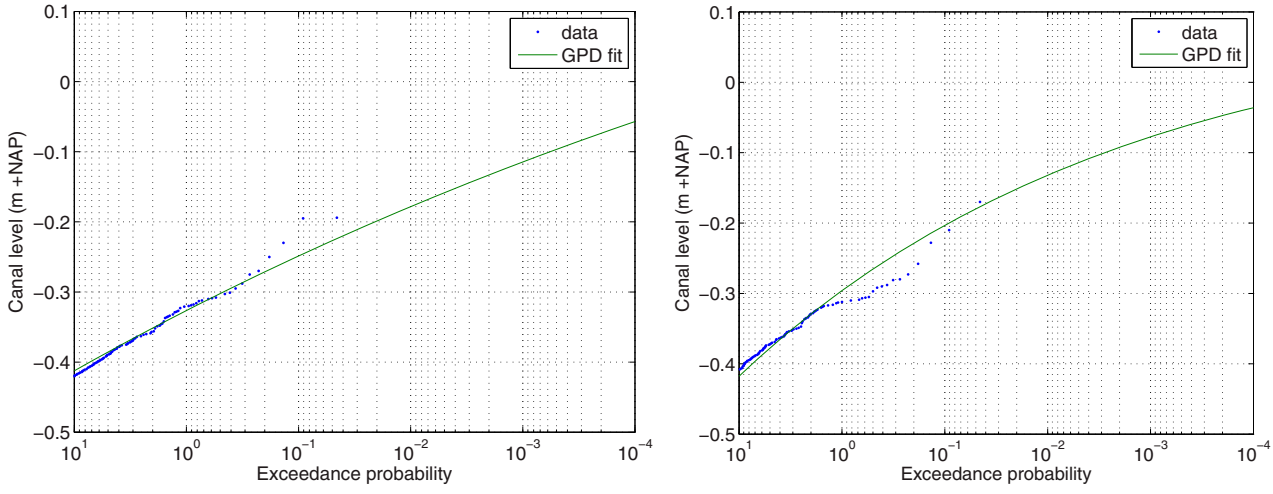

Figure 6. GDPs fitted to independent water level peaks at Heerhugowaard (left) and Wogmeer (right) station.

Table 1. Probability of water levels exceeding the drainstop level.

Location	Canal	Target level [m NAP]	Drainstop level [m NAP]	Frequency $h >$ drainstop [yr^{-1}]	Probability ($h >$ drainstop) [yr^{-1}]
Heerhugowaard	Schermer	−0.5	0	0	0.01 (1/100)
Wogmeer	VRNK	−0.6	−0.3	0.1303	0.1144 (1/9)

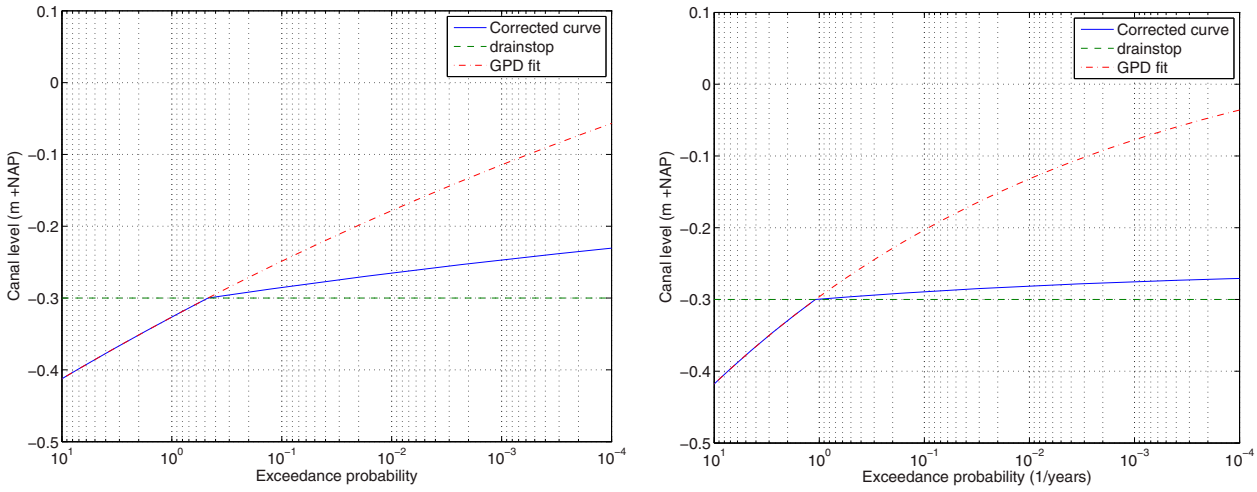

Figure 7. Annual exceedance frequency model of Heerhugowaard (left) and Wogmeer (right) pumping station.

We assume that a low or high phreatic surface, given an average water level in the canal, has equal probability of 1/100. This estimate is based on the probability of exceedance of the drainstop level in the canal. As explained, this scenario represents the likelihood of events that cause the canal water levels to reach the drainstop level. The remaining probability mass for the average phreatic surface level is 98/100.

- Given extreme canal water levels: with water levels in the canal reaching the drainstop level, it is most likely that the phreatic surface is high (and the levee saturated). Both an increase in the canal water level and the phreatic surface are caused by the same driver: precipitation. Therefore, we estimate the probability of a low and an average phreatic surface, given extreme canal water levels, to be 1/100. The remaining probability mass for the high phreatic surface level is 98/100.

The results are summarised in the conditional probability table (Table 2).

3.2.3. Traffic load

Regional water board employees responsible for the operation and maintenance of canal levees were asked to provide estimates of the 5th, 50th and 95th quantiles of the statistical distribution of the traffic load, based on the weight of vehicles that are allowed on top of the levees. These estimates were used to generate a triangular PDF. The results are presented in Figure 8. Compared to the deterministic value of the traffic load (13.3 kN/m), a higher expected value is found: 16.5 kN/m^2. Experts explained that the weight of the assumed design vehicle is underestimated (Stowa 2007), which is why they estimated the traffic load to be higher than the guidelines propose.

The regional water board employees all agreed that traffic loads can be expected during average situations, but had different views on whether or not traffic loads on canal levees can be expected during extreme situations (e.g. when the water level is at the drainstop level). Some argue that during extreme events, flood

Table 2. Conditional probability table of canal water level and phreatic surface.

		Phreatic Surface level		
		Low phreatic surface	Average Phreatic Surface	High Phreatic Surface
Canal water level	Low water level	0.01	0.98	0.01
	Average water level	0.01	0.98	0.01
	High water level	0.01	0.01	0.98

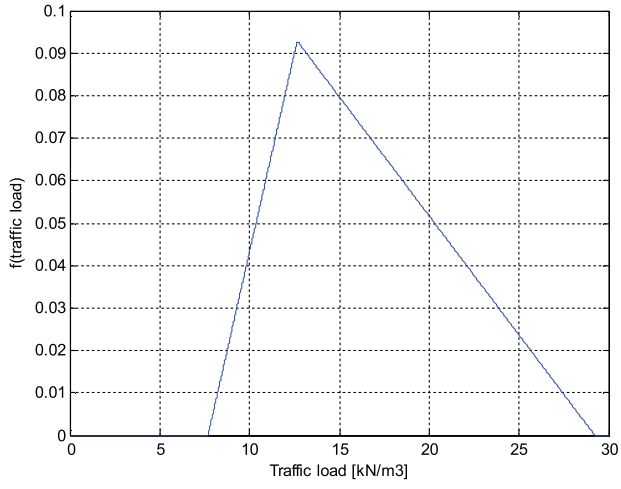

Figure 8. Triangular distribution of traffic load on canal levees in the Heerhugowaard.

fighting will take place, resulting in considerable traffic loads on the levee, while others argue that no traffic is allowed in this situation to avoid instability of the levee. To understand the impact of traffic loads on the probability of instability, in the "base case" we calculate the conditional probability of failure of the levee and assume a probability of 1/2 for the presence of traffic loads (P_{tl}). In addition, with sensitivity analyses, we will also estimate the probability of failure for situations with different probabilities of traffic loads.

3.3. Application and results

This paragraph discusses the results of the failure probability assessment for Section 4 in reach 1 of the case study. This section is situated along the VRNK canal near the Wogmeer pumping station (Figure 5). Assumptions regarding case-specific parameters used in the probabilistic calculations are included in each subsection. Details regarding piping input parameters are included in the supplement.

3.3.1. Overflow

The resistance against overflow is determined by the retaining height (crest level) of the canal levee and the resistance to erosion of the inner slope. The input variables are shown in Table 3. The critical overflow amount depends on the overflow resistance of the inner slope cover layer. According to the guidelines (Stowa 2007), a maximum amount of 0.1 L/m/s is allowed. However, recent tests have proved that well-developed grass cover layers can resist much more (EurOtop 2007). A deterministic critical overflow amount of 5 L/m/s is assumed, leading to a critical overflow height of 0.02 m according to Equation (9).

The annual probability of overflow of the considered section is estimated smaller than 1/10.000. This low value is explained by the retaining height of the canal levee, which lies well above canal water levels and corresponds to water levels with annual exceedance probabilities below 1/10.000 (see Figure 7). These low exceedance probabilities are explained partly by the low probability of exceedance of the drainstop level. The corresponding fragility curve is shown in Figure 9.

Table 3. Input variables overflow for Section 4.

Variable	Parameter	Distribution	Mean	Standard deviation
Crest level	H_r	Normal	0.38 m	0.038 m
Critical flow	q_c	Deterministic	$5{\cdot}10^{-3}$ m^3/s	–
Critical overflow height	Δh_c	Deterministic	$2.0{\cdot}10^{-2}$ m	–

3.3.2. Piping

The probability of piping depends on the amount of hydraulic resistance (H_{ir}) and the probability of (accidental) removal of hydraulic resistance due to dredging activities ($P_{\overline{ir}}$). The specific input parameters for Section 4 are shown in Table 4, the remaining parameters used in the calculation are included in the supplement.

The probability of piping ($P_{f;p}$) conditional on the probability of removal of hydraulic resistance ($P_{\overline{ir}}$) is determined through Monte Carlo simulation, using the annual exceedance frequency model of Wogmeer station. Figure 10 illustrates the conditional probability of piping, which increases with increasing probability of removal of hydraulic resistance due to dredging ($P_{\overline{ir}} = 1 - P_{ir}$).

The conditional annual probability of piping varies between a probability of 0.005 and 0.034, depending on the probability of removal of the hydraulic resistance. The VRNK canal is dredged every year. We assume a probability of (accidental) removal of the impermeable layer during maintenance dredging of 1/10 per dredging activity, which is common for activities subject to human error (Bea 2010). The resulting annual probability of removal of hydraulic resistance ($P_{\overline{ir}}$) is 1/10. The annual probability of piping for Section 4 can now be calculated using Equation (11) and amounts to 0.082, or 1/13. The

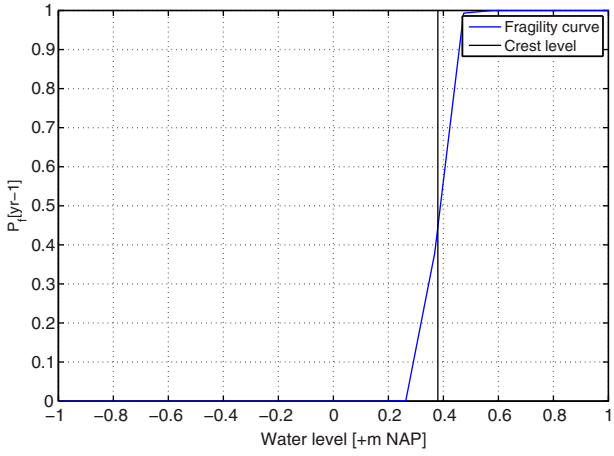

Figure 9. Overflow fragility curve (Section 4).

Table 4. Specific input variables piping for Section 4.

Variable	Parameter	Unit	Distribution	Mean (μ)	Coefficient of variation (CV)
Model parameter	m_b	–	LogNormal	1	0.12
Thickness of blanket layer	D_0	m	LogNormal	0.3	0.1
Polder level	H_i	m NAP	Normal	−3.9	0.1
Hydraulic resistance	H_{ir}	M	LogNormal	2.7	0.22

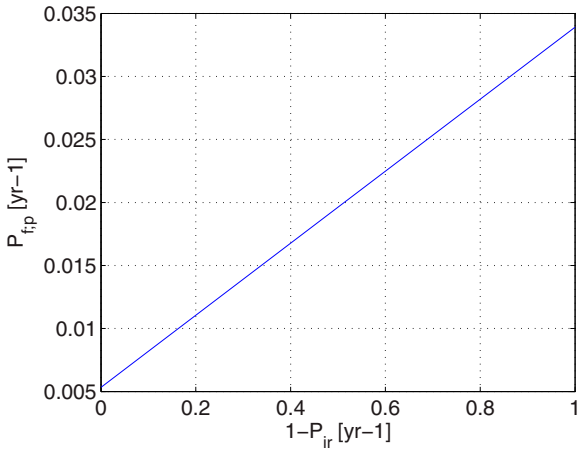

Figure 10. Piping failure probability conditional on probability of removal of hydraulic resistance (Section 4).

corresponding fragility curve for piping is shown in Figure 11.

The probability of piping is rather high given the fact that no signs of piping (e.g. heave or uplifting) have been observed along the canal levee during the last decades. Performance observations are used to further refine the probability of piping, using evidence of survived loads. The strength properties of piping lie in the geotechnical properties of the aquifer under the levee (e.g. the permeability and thickness of the aquifer and the seepage length of the levee). We assume the geotechnical properties of the survived event and the current situation to be perfectly correlated because no large changes to (the geotechnical properties of) the levee have occurred in the period between the survived load until the current situation. A stepwise description of the method used is found in Schweckendiek, Vrouwenvelder, and Calle (2014).

The highest observed water level in the VRNK canal is used in the posterior analysis. Due to the lack of information of dredging during the observed water level, we assume that the impermeable layer on the bottom of the canal was present during the survived load. This load case is defined as load case *h*1, see Table 5.

The *a-posteriori* probability of piping given survival of load case *h*1 is calculated with Equation (13). The survival of load case *h*1 results in a reduction of the annual probability of piping to a range of $<10^{-5}$ and 0.026, as can be seen in Figure 12. Assuming an annual probability of removal of the hydraulic resistance due to dredging of 1/10, we find an annual probability of piping of 0.0027.

Suppose that that the impermeable layers on the bottom of the canal were removed right before the survived load occurred, resulting in the absence of hydraulic resistance. The hydraulic head during this hypothetical load case, defined as *h*2 (see Table 5), is significantly higher than the average hydraulic head over the levee (in the order of several metres) in daily circumstances, due to the absence of hydraulic resistance. The conditional annual probability of piping given load case *h*2 ($P_{f;\text{posterior}|h2}$) is smaller than 10^{-5} as shown in Figure 12. The resulting probability of piping is more realistic for the considered dike section considering the absence of signs of piping. However, we cannot exclude the possibility of no hydraulic resistance during the survived

Table 5. Properties of load cases for posterior analysis of piping.

	Survived water level (H_s)	Mean of hydraulic resistance (H_{ir})
Load case *h*1	−0.17 m NAP	2.7 m
Load case *h*2	−0.17 m NAP	0 m

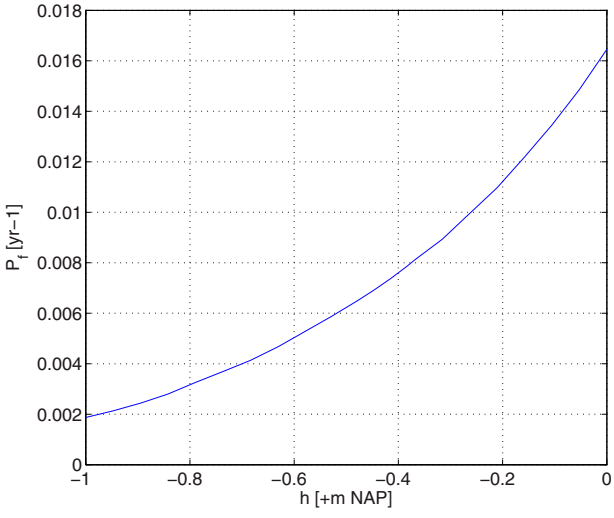

Figure 11. Piping fragility curve given an annual probability of removal of hydraulic resistance of 1/10 (Section 4).

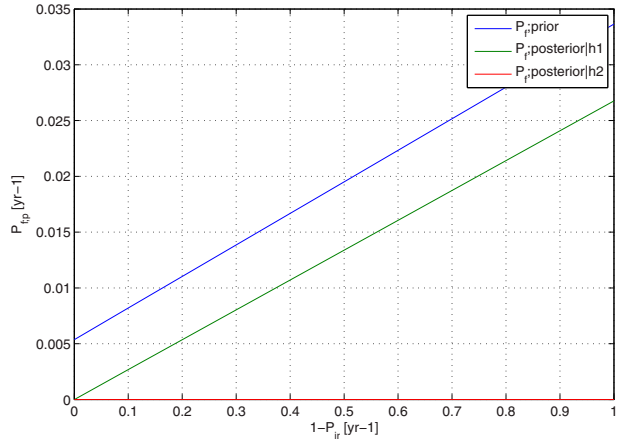

Figure 12. The *a-priori* conditional probability of piping ($P_{f;\text{prior}}$), *a-posteriori* probability given load case *h*1 ($P_{f;\text{posterior}|h1}$) and load case *h*2 ($P_{f;\text{posterior}|h2}$).

load, because we do not know the conditions during the survived load. We therefore conclude that the probability of piping is determined by the *a-posteriori* probability given load case *h*1 and an annual probability of removal of hydraulic resistance of 1/10. This results in an annual probability for piping of (0.026·0.1 + 10^{-5}·0.9) 0.0026, or 1/384. Figure 13(a) illustrates the fragility curve of the *a-priori* probability of piping, the *a-posteriori* probability given load case *h*1 and load case *h*2.

The probability of piping is dominated by the conditional annual probability of piping given no hydraulic resistance (0.026). This study assumed an annual probability of removal of the hydraulic resistance of 1/10. Reduction of this probability will reduce the probability of piping. Furthermore, load case *h*2 demonstrated that the probability of piping can be further reduced using a test load on the canal levee, consisting of the removal of the impermeable layer on the bottom of the canal and raising the water level in the canal.

3.3.3. Inner slope instability

The stability of the inner slope depends on three loads: (i) the water levels in the canal, (ii) the phreatic surface in the levee and (iii) the traffic load on top of the levee. Cross sections of the schematised canal levee in D-Geo Stability are shown in Figure 14. The illustrated schematisation shows a canal levee with a phreatic surface representative for a steady state situation, conditional on the canal water level. The conditional probability of inner slope instability is calculated with D-Geo Stability for several deterministic combinations of these loads, the results are included in Table 6.

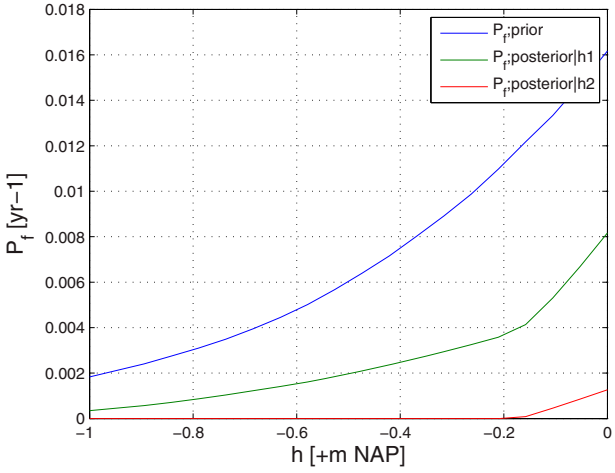

Figure 13. Piping fragility curves for the *a-priori* failure probability, the *a-posteriori* probability given load case *h*1 and load case *h*2. Each load case considers an annual probability of removal of hydraulic resistance of 1/10.

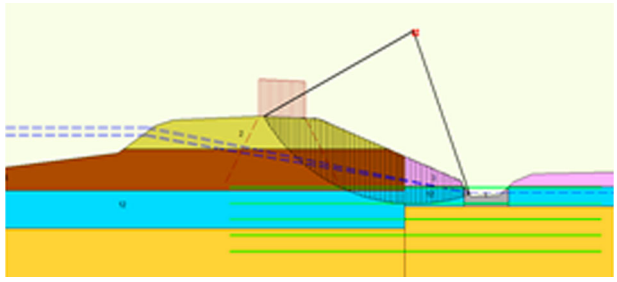

Figure 14. Cross section of schematisation of Section 4 in D-Geo Stability showing the canal water level, the phreatic surface and traffic loads. Also displayed is a slip circle that would lead to breaching. The influence of the canal water levels on the canal-side boundary of the phreatic surface level can be seen in the figure.

The results show that increasing water levels have a negligible effect on the probability of failure for a low and an average phreatic surface (specifically within the estimated slip circles of the inner slope, see Figures 15 and 16. In contrast, for a high phreatic surface, increasing water levels in the canal do result in increasing probabilities of failure. This is also visible in the fragility curves illustrated in Figures 15 and 16. The figure illustrates the probability of failure conditional on each load after integration over the joint probability distribution function of the remaining loads. For example, the fragility curve to the left illustrates the failure probability conditional on the water levels after integration over the conditional probabilities of the phreatic and the traffic load (illustrated in Figure 8). Specifically, the scenario with extreme water levels (near or over the

Table 6. Annual probability of instability for combinations of water level and phreatic surface given a deterministic traffic load (Section 4).

Water level (m NAP)	Low	Average	High
Traffic load = 0 kN/m²			
−0.67 m NAP	$1.3{\cdot}10^{-8}$	$2.5{\cdot}10^{-8}$	0.008
−0.59 m NAP	$1.3{\cdot}10^{-8}$	$2.5{\cdot}10^{-8}$	0.009
−0.30 m NAP	$1.3{\cdot}10^{-8}$	$2.5{\cdot}10^{-8}$	0.015
−0.17 m NAP	$1.3{\cdot}10^{-8}$	$2.5{\cdot}10^{-8}$	0.019
Traffic load = 5 kN/m²			
−0.67 m NAP	$2.4{\cdot}10^{-8}$	$4.4{\cdot}10^{-8}$	0.011
−0.59 m NAP	$2.4{\cdot}10^{-8}$	$4.4{\cdot}10^{-8}$	0.019
−0.30 m NAP	$2.4{\cdot}10^{-8}$	$4.4{\cdot}10^{-8}$	0.024
−0.17 m NAP	$2.4{\cdot}10^{-8}$	$4.4{\cdot}10^{-8}$	0.024
Traffic load = 13 kN/m²			
−0.67 m NAP	$1.2{\cdot}10^{-7}$	$2.1{\cdot}10^{-7}$	0.018
−0.59 m NAP	$1.2{\cdot}10^{-7}$	$2.1{\cdot}10^{-7}$	0.022
−0.30 m NAP	$1.2{\cdot}10^{-7}$	$2.1{\cdot}10^{-7}$	0.038
−0.17 m NAP	$1.2{\cdot}10^{-7}$	$2.1{\cdot}10^{-7}$	0.048
Traffic load = 30 kN/m²			
−0.67 m NAP	$5.0{\cdot}10^{-7}$	$8.8{\cdot}10^{-7}$	0.033
−0.59 m NAP	$5.0{\cdot}10^{-7}$	$8.8{\cdot}10^{-7}$	0.039
−0.30 m NAP	$5.0{\cdot}10^{-7}$	$8.8{\cdot}10^{-7}$	0.068
−0.17 m NAP	$5.0{\cdot}10^{-7}$	$8.8{\cdot}10^{-7}$	0.087

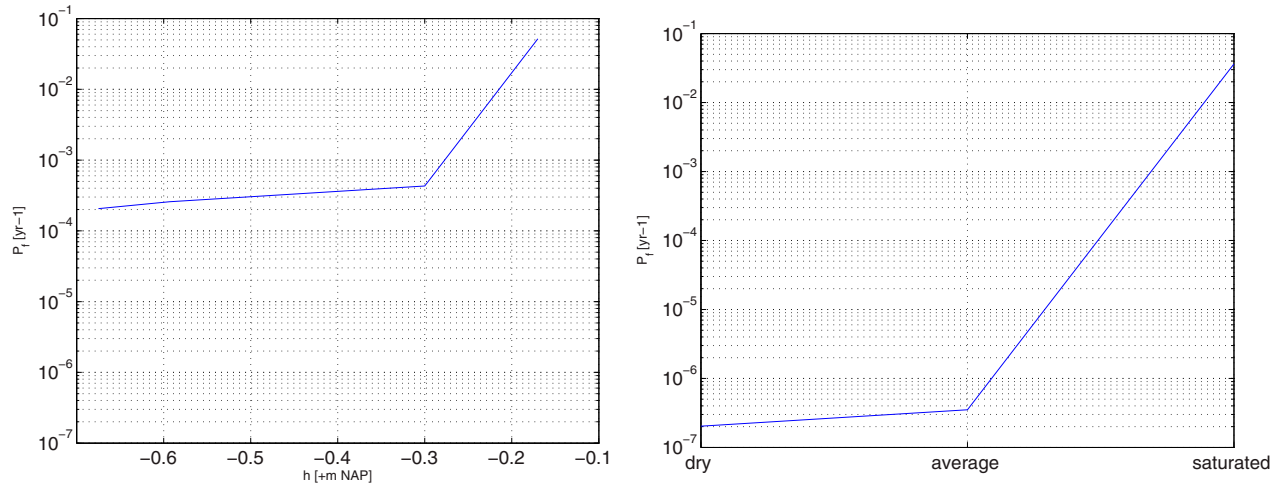

Figure 15. Fragility curves for inner slope instability conditional on the canal water level (left) and the phreatic surface (right).

drainstop level), combined with a saturated levee due to a high phreatic surface, result in the highest conditional probability of failure.

Given the estimates of the water board employees regarding traffic loads (see Section 2.3.3), we assume that traffic load on top of the levee is independent of the occurring hydraulic loads. The conditional failure probabilities are subsequently integrated over the probability distribution function of each load as defined in the "base case" and summed. The results are shown in Table 7. Figure 17 illustrates the sensitivity of the probability of instability on the probability of traffic loads.

Sensitivity analyses were also performed to study the impact of the estimates of the conditional probability table of the phreatic surface and the probability of traffic loads. In the base case, the probability of a phreatic surface other than the level most likely to occur given a certain water level was estimated at 1/100. This value was varied between 1/10 and 1/1000 to study the sensitivity of the probability of instability to this value. The results are shown in Table 8. A reduction of the probability of "other" phreatic surfaces does not to have a large effect. An increase with an order of magnitude results in a larger difference, but probabilities remain within the same order of magnitude. Thus, the sensitivity to these assumptions is not very large.

Performance observations can be used to further refine the probability of instability, using evidence of survived loads (Schweckendiek and Vrouwenvelder 2013).

Table 7. Annual probability of inner slope instability conditional on the presence of traffic loads, for the "base case".

	Parameter	Value
Probability of inner slope instability without traffic loads	$P_{f;\text{inst}\|\overline{\text{tl}}}$	$1.5{\cdot}10^{-3}$
Probability of inner slope instability with traffic loads	$P_{f;\text{inst}\|\text{tl}}$	$4.0{\cdot}10^{-3}$

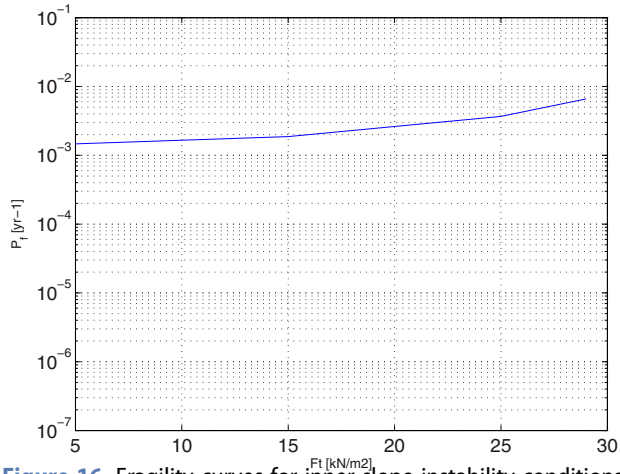

Figure 16. Fragility curves for inner slope instability conditional on the traffic load.

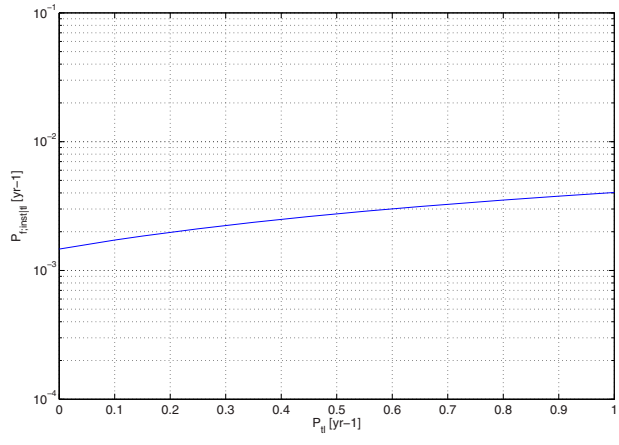

Figure 17. Annual probability of inner slope instability conditional on the presence of traffic loads, for the "base case".

Initiation of instability failure can be observed by movements of the levee in downstream direction, causing cracks in the levee. Such signs of failure/performance can be incorporated in a Bayesian Analysis, similar to what was done for piping. The formation of cracks could be considered as an initiated slope failure within the analysis used to update the estimated prior failure probabilities.

The strength properties of the instability failure mechanism are determined by both the geometrical and geotechnical properties of the levee. Similar to the piping mechanism, we can assume that these properties are highly correlated between the survived event and the predicted (future) event, if we can exclude the possibility of large changes over time. However, posterior analyses only have a large impact on the probability of failure if the water level in the canal is dominant over other loads. The results of this study demonstrated that the phreatic surface, influenced by precipitation, is dominant. Therefore, performing a similar posterior analysis for instability as done for piping may not have a large impact on the probability of failure, because insight is required in the level of the phreatic surface at the time of the survived load.

3.3.4. Probability of failure

The annual probability of each failure mechanism for the considered dike section is summarised in Table 9. Failure probabilities are combined assuming independence between the failure mechanisms, to obtain an estimate of the annual probability of failure of the considered dike section, according to Equation (9). When comparing the probabilities of the failure mechanisms, we conclude that the geotechnical failure mechanisms (i.e. piping and instability) are dominant. These results substantiate the assumption about independence between failure mechanisms.

The resulting annual probability of failure of the considered section is 1/200. This paper has demonstrated the assessment of probabilities of failure of one dike section. To assess probabilities of failure on system level we need to consider the length-effect within homogeneous sections as well as the system reliability when combining the various sections in the system, which essentially work as a parallel system. Methods that can be used for this purpose are explained in Kanning (2012).

Table 8. Sensitivity analyses showing the impact of varying conditional probabilities of the phreatic surface.

	Parameter	Value
Probability of inner slope instability, probability of "other" phreatic surface of 1/100 (base case)	$P_{f;inst}$	$2.7{\cdot}10^{-3}$
Probability of inner slope instability, probability of "other" phreatic surface of 1/1000	$P_{f;inst}$	$2.6{\cdot}10^{-3}$
Probability of inner slope instability, probability of "other" phreatic surface of 1/10	$P_{f;inst}$	$4.3{\cdot}10^{-3}$

Note: Here, the "other" phreatic surfaces are defined as the levels that are not most likely to occur given a certain water level.

Table 9. Annual probabilities of failure for Section 4 of case study.

Failure mechanism	Parameter	Value
Overflow	$P_{f;o}$	<0.000001 (1/100,000)
Piping (with performance observations)	$P_{f;p}$	0.0026 (1/384)
Instability	$P_{f;inst}$	0.0027 (1/370)
Probability of failure	P_f	0.005 (1/200)

4. Concluding remarks

This paper proposes an approach to quantify the probability of failure of a canal levee, based on the probabilistic methods developed for flood defences along the main water bodies. In our approach, the continuous PDFs of several load variables are discretized in a predefined set of plausible load levels with corresponding probability density. The total law of probability was used to account for (i) regulation (and drainstop) of water levels in canals, (ii) maintenance dredging and its influence on the hydraulic resistance of the canal, (iii) the uncertain presence of traffic loads and (iv) the uncertainty of the phreatic surface. In addition, reliability updating is used to demonstrate the impact of incorporating performance observations for the piping failure mechanism.

The proposed approach was applied to a case study of a canal levee system in the Netherlands. The probability of three failure mechanisms was determined: overflow, piping and instability. The probability of overflow was dominated by the probability of drainstop failure. For piping, the probability of failure was largely influenced by the (probability of) hydraulic resistance of the bottom layer of the canal. A posterior analysis demonstrated the ability to reduce the probability of piping using performance observations. The posterior analysis opens opportunities for testing the piping resistance of a canal levee under different combinations of loads.

The probability of instability of the inner slope was dominated by the uncertainty in the phreatic surface and traffic loads. We conclude that the probability of failure of the considered dike section is governed by the probability of piping and instability. The probability of overflow is negligible.

Based on the results of this paper, we recommend further investigating dependencies between canal water levels and the phreatic surface, also taking into account system size and capacity, and the potential of

incorporating performance observations in the quantification of the probability of instability of the inner slope.

Overall, we conclude that the proposed approach can be used to quantify the probability of failure of canal levees. By doing so, the approach contributes to improving flood management of canal levee systems by providing input for risk assessments of canal levee systems. With these methods, it becomes possible to evaluate and prioritise different flood risk reduction measures (e.g. levee reinforcement or increasing drainage capacity) in terms of their costs and benefits (or risk reduction).

Acknowledgements

HHNK are thanked for their cooperation during the project. In addition, Professor S.N. Jonkman is thanked for his useful comments and support during the project.

Disclosure statement

No potential conflict of interest was reported by the authors.

Funding

The authors would like to express their gratitude to STOWA, (the research foundation of the Dutch water boards) for their financial support.

References

Bea, R. 2010. *Human & Organizational Factors : Risk Assessment & Management of Engineered Systems Proactive*. Berkeley, CA: University of Berkeley.

Bishop, A. W. 1955. "The Use of the Slip Circle in the Stability Analysis of Slopes." *Geotechnique* 5: 7–17.

Ciria. 2014. *The International Levee Handbook*. 1st ed. London: Ciria.

Deltares. 2016. *D-Geo Stability User Manual*. Delft: Deltares.

ENW. 2009. *Technisch Rapport: Actuele Sterkte van Dijken*. Delft: ENW.

EurOtop. 2007. *Wave Overtopping of Sea Defences and Related Structures: Assessment Manual*. Utrecht: Envrionment Agency, ENW, KFKI.

Gouldby, B., P. Sayers, J. Mulet-Marti, M. A. A. M. Hassan, and D. Benwell. 2008. "A Methodology for Regional-Scale Flood Risk Assessment." *Proceedings of the Institution of Civil Engineers - Water Management* 161 (3): 169–182.

Jongejan, Ruben, B. Maaskant, and W. Ter Horst. 2013. "The VNK2-Project: A Fully Probabilistic Risk Analysis for All Major Levee Systems in the Netherlands." *IAHS*. Accessed May 16, 2014. http://www.hkvconsultants.de/documenten/The_VNK2_project_a_fully_probabilistic_risk_etc_BM_FH(2).pdf.

Jonkman, S. N. 2005. "Global Perspectives on Loss of Human Life Caused by Floods." *Natural Hazards* 34: 151–175.

Jonkman, S. N., and M. Kok. 2008. "Risk-Based Design of Flood Defence Systems – A Preliminary Analysis for the New Orleans Metropolitan Area." 4th International Symposium on Flood Defence: Managing Flood Risk, Reliability and Vulnerability, Toronto, Ontario, Canada, May 6–8, 31-1–31-9. Accessed November 20, 2013. http://www.hkvlijninwater.nl/documenten/Risk-based_design_of_flood_defence_systems_WEBSITE_MK.doc.pdf.

Kanning, Wim. 2012. *The Weakest Link: Spatial Variability in the Piping Failure Mechanism of Dikes*. Delft: TU Delft.

Kirwan, B. 1996. "The Validation of Three Human Reliability Quantification Techniques—THERP, HEART and JHEDI: Part 1—Technique Descriptions and Validation Issues." *Applied Ergonomics* 27 (6): 359–373. Accessed November 20, 2013. http://www.ncbi.nlm.nih.gov/pubmed/15677076.

Lendering, K. T., S. N. Jonkman, and M. Kok. 2015. "Effectiveness of Emergency Measures for Flood Prevention." *Journal of Flood Risk Management* 9: 320–334.

Lendering, K. T., M. Kok, and S. N. Jonkman. 2015. *Flood Risk Regional Flood Defences*. Amersfoort: STOWA.

Rijkswaterstaat. 2015. *Deltaprogramma 2015: Werk Aan de Delta*. Den Haag: Rijkswaterstaat.

Schweckendiek, T. 2014. *On Reducing Piping Reliabilities: A Bayesian Decision Approach*. Delft: Delft University of Technology.

Schweckendiek, T., and A. C. W. M. Vrouwenvelder. 2013. "Reliability Updating and Decision Analysis for Head Monitoring of Levees." *Georisk: Assessment and Management of Risk for Engineered Systems and Geohazards* 7 (2): 110–121.

Schweckendiek, T., A. C. W. M. Vrouwenvelder, and E. O. F. Calle. 2014. "Updating Piping Reliability with Field Performance Observations." *Structural Safety* 47: 13–23. Accessed January 10, 2014. http://linkinghub.elsevier.com/retrieve/pii/S0167473013000799.

Sellmeijer, Hans, Juliana López de la Cruz, Vera M. van Beek, and Han Knoeff. 2011. "Fine-Tuning of the Backward Erosion Piping Model through Small-Scale, Medium-Scale and IJkdijk Experiments." *European Journal of Environmental and Civil Engineering* 15 (8): 1139–1154.

Slijkhuis, K. A. H., P. van Gelder, and J. K. Vrijling. 2001. "Optimal Dike Height Under Statistical-, Construction-and Damage Uncertainty." *Citg.tudelft.nl* 7: 1137–1140. Accessed November 20, 2013. http://www.citg.tudelft.nl/fileadmin/Faculteit/CiTG/Over_de_faculteit/Afdelingen/Afdeling_Waterbouwkunde/sectie_waterbouwkunde/people/personal/gelder/publications/papers/doc/paper12.pdf.

Stowa. 2007. *Leidraad Toetsen Op Veiligheid Regionale Waterkeringen*. Utrecht: STOWA.

Van Baars, S., and I. M. Van Kempen. 2009. "The Causes and Mechanisms of Historical Dike Failures in the Netherlands." *E-WAter* 2009 (6): 1–14. http://www.ewa-online.eu/e-water-documents.html.

Van Esch, John M. 2012. "Modeling Groundwater Flow Through Embankments for Climate Change Impact Assessment." 1–10.

Vorogushyn, S., B. Merz, and H. Apel. 2009. "Development of Dike Fragility Curves for Piping and Micro-Instability Breach Mechanisms." *Natural Hazards and Earth System Science* 9: 1383–1401.

Vrijling, J. K. 2001. "Probabilistic Design of Water Defense Systems in the Netherlands." *Reliability Engineering & System Safety* 74 (3): 337–344. Accessed November 20, 2013. http://www.sciencedirect.com/science/article/B6V4T-4475SXJ-D/2/67b27fa241ab41a3fbfb45669a961cc4.